Macromolecules

ARTICLE

pubs.acs.org/Macromolecules

Crystallization Behavior of Carbon Nanotube−Polylactide Nanocomposites

S. Barrau,*,† C. Vanmansart,† M. Moreau,‡ A. Addad,† G. Stoclet,† J.-M. Lefebvre,† and R. Seguela†

†Unité Matériaux et Transformations (UMET), CNRS UMR 8207, Université Lille 1, Sciences et Technologies, 59655 Villeneuve d'Ascq, France

‡Laboratoire de Spectrochimie Infrarouge et Raman (LASIR), CNRS UMR 8516, Université Lille 1, Sciences et Technologies, 59655 Villeneuve d'Ascq, France

ABSTRACT: The crystallization kinetics and the resulting structure and morphology of polylactide (PLA) were investigated in the presence of carbon nanotubes (CNTs). Nanocomposite samples prepared by solution and melt mixing present homogeneous filler dispersion, as observed by scanning electron microscopy. Calorimetric characterization of the nonisothermal and isothermal crystallization behavior analyzed according to Avrami's theory provides evidence of the significant impact of CNTs on the crystallization kinetics of the PLA matrix. The nucleating effect of the nanofillers is confirmed by Raman spectroscopy experiments. Indeed, during isothermal crystallization, the nanotube characteristic vibrations are strongly affected by the development of polymer crystalline phase. Additionally, CNTs increase the number of nucleation sites and thereby decrease the average spherolite size as observed by optical microscopy. The PLA crystal structure is not modified by the presence of CNTs, as probed by X-ray diffraction.

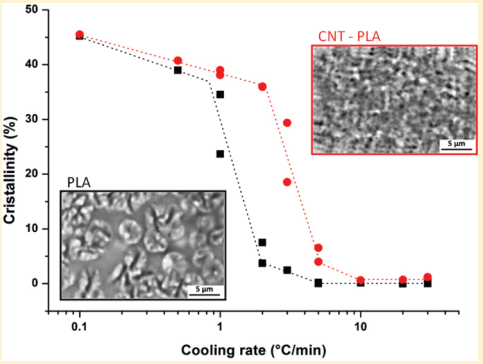

1. INTRODUCTION

Environmentally friendly polymers such as polylactide (PLA) have attracted increasing interest in the past decades. PLA is not only biodegradable[1] but also produced from renewable resources,[2] which is an alternative to the exhaustion of petroleum resources. PLA is a linear, aliphatic polyester mainly used in biomedical or in film packaging applications. However, with an increasing production capacity, PLA is potentially interesting for further developments (mechanical, electronics, etc.) requiring specific performances. A well-known approach for improving physical and mechanical properties[3] is to introduce nanofillers. The resulting nanocomposite material may present a synergistic effect of the two components, leading to considerable improvement of various properties, with respect to the neat polymer material. For this purpose, pristine clays,[4] organically modified clays,[5−9] fibers,[10] whiskers,[11] or more recently carbonaceous fillers[12−14] have received considerable attention. Carbon nanotubes (CNTs), which exhibit excellent physical properties in addition to nanometer dimensions, appear as excellent candidates to make advanced functional composite materials[15−17] even if they are not adapted to the elaboration of environmentally friendly composites. The efficiency of CNTs depends on their intrinsic properties but also on structural characteristics such as dispersion and alignment and interfacial properties as well. However, since CNTs usually form stabilized bundles due to van der Waals interactions, dispersion in a polymer matrix is extremely difficult. Monitoring and assessing filler dispersion therefore remains one of the biggest issues in the preparation of CNT-reinforced nanocomposites.[18]

Considering that PLA is a semicrystalline polymer,[19,20] its mechanical and physical properties are governed by the supermolecular morphology, which is in turn controlled by the crystallization process. Reinforcement at the nanoscale in order to improve polymer properties is expected to change the PLA crystallization behavior.[21−23] CNTs interactions with the semicrystalline polymer host may potentially alter the crystallization kinetics and the crystalline morphology of the latter.[24,25] For instance, CNTs act as nucleating agents for polypropylene crystallization.[26] Haggenmueller et al.[27] showed that CNTs nucleate polyethylene crystals and accelerate the crystallization rate. Lamellae grow perpendicular to the nanotube surface and CNT orientation dictates the polymer orientation. Brosse et al.[28] provide evidence of the presence of transcrystalline lamellae on the CNT surfaces in polyamide 6 nanocomposites, with a polymer crystallographic lattice matching that of nanotubes.

In the present study we investigate the effect of CNTs on the crystallization kinetics of a PLA matrix. Considering that nanofillers often promote crystallization of the polymer matrix via nucleation at low content, but also impede crystal growth at higher content,[29,30] two types of nanocomposites with CNT contents 0.1 and 1 wt % were prepared. Raman spectroscopy is used as a complementary tool to conventional calorimetric techniques in

Received: April 12, 2011
Revised: July 7, 2011
Published: July 28, 2011

order to achieve in-situ monitoring of the polymer crystallization process from the study of CNT vibration bands.

2. EXPERIMENTAL SECTION

2.1. Materials and Composite Elaboration. The polylactide purchased from Natureworks (4042D grade) is a copolymer containing 4.3% of D-isomer. Its number- and weight-average molar weights are M_n = 116 000 g/mol and M_w = 188 400 g/mol, respectively. Multiwalled carbon nanotubes produced from the catalytic carbon vapor deposition (CCVD) process were obtained from Nanocyl (Nanocyl7000 series, Belgium). The average diameter and length are 9.5 nm and 1.5 μm, respectively. The batch contains 10 wt % of oxidized catalytic residues, mainly alumina.

The nanocomposites were elaborated in two steps, first by solution mixing in order to disaggregate the CNTs and then by melt processing of the dried mixture to overcome partial sedimentation from the solution mixing and to obtain a homogeneous dispersion of the nanofillers in the polymer matrix. The elaboration protocol was the following. CNTs were dispersed in THF and sonicated for 1 h at ambient temperature. PLA was then added to the solution that was magnetically stirred at 50 °C for 2 h. The CNT/PLA ratio was calculated to produce nanocomposites with 0.1 and 1 wt % CNT contents. The solution was subsequently poured into silicone cups in order to allow solvent evaporation at room temperature under atmospheric pressure for one night. The residual solvent was removed by placing the composites in a vacuum oven at 160 °C for 30 min. The "dried" material was then melt-compounded using a twin-screw microextruder from DSM Xplore (Geelen, The Netherlands) operated at 180 °C, at a screw speed of 50 rpm, and for a residence time of 5 min under a nitrogen atmosphere. The extrudates were cooled in air at the exit of the die having a 2 mm diameter. For comparison, the neat PLA sample was also processed under similar conditions combining solution mixing and melt processing, in order to ensure identical thermal history. The composites are denoted NT*x*, where *x* holds for the CNT content in wt %, namely NT0 for neat PLA, NT01 and NT1 for composites with 0.1 and 1 wt %, respectively.

2.2. Experimental Techniques. *Scanning Electron Microscopy.* The morphology of nanocomposites was investigated by field emission scanning electron microscopy (FE-SEM) using an Hitachi S4700 apparatus operated at an acceleration voltage of 6 kV. The micrographs were taken from the surface of cryofractured samples previously coated with carbon.

Differential Scanning Calorimetry. Thermal characterization of PLA and composites was performed with a DSC7 Perkin-Elmer instrument calibrated with indium under a nitrogen atmosphere. Aluminum sample pans with ~3 mm diameter were used for all samples. The crystalline thermal history of the polymer was erased by heating the samples at 180 °C for 5 min.

The same samples were used for both nonisothermal and isothermal crystallization experiments. For nonisothermal crystallization experiments, the composites underwent cooling at a controlled rate (from 30 to 0.1 °C/min) to ambient temperature, followed by a heating scan at 20 °C/min up to 180 °C. For isothermal crystallization experiments, the composites were quenched at a controlled rate of 40 °C/min to the chosen isothermal crystallization temperature T_c (from 90 to 120 °C) and held at T_c for 60 min. The samples were then quenched to ambient temperature and heated to 180 at 20 °C/min. The crystallinity was determined from the relation $X = \Delta H_f/\Delta H_f^0$, where ΔH_f^0 = 93 J/g is the melting enthalpy of 100% crystallized polylactide.[31]

Polarized Optical Microscopy. An Olympus AX70 microscope equipped with a temperature-controlled hot-stage was used in transmission mode to study the morphology. The samples were heated from room temperature to 180 °C, held 5 min for melting of the polymer, rapidly cooled to the desired crystallization temperature, and then maintained at T_c until crystallization completion.

Wide-Angle X-ray Scattering. Measurements were performed by wide-angle X-ray scattering (WAXS) at room temperature on samples beforehand crystallized from solid state at 120 °C for 2 h. The X-ray source was generated by a 1.5 kW sealed tube with Cu target (λ = 1.54 Å), operated at 20 mA and 40 kV. The sample-to-detector distance was 6 cm. 2D-WAXS patterns were recorded on a CCD camera from Photonic Science Ltd. Radial WAXS intensity profiles were obtained by azimuthal integration using the FIT2D software.[32]

ESRF Wide-Angle X-ray Scattering. Complementary WAXS measurements were carried out on the BM02 beamline at the European Synchrotron Radiation Facility (ESRF, Grenoble, France) equipped with a 0.5 mm point-focusing collimation and using an X-ray energy of 24 keV (λ = 0.51 Å). Corrections were applied for background scattering, geometry, and intensity distortions of the detector (Roper Scientific PI SCX90-1300 model). In-situ temperature measurements were performed with an hot-stage thermal control unit from the melt state (180 °C) to ambient temperature at a cooling rate of 5 °C/min.

Raman Spectroscopy. The Raman spectra were obtained using a LabRam HR (Horiba Jobin Yvon) system. The excitation source is a 532 nm laser for which power at the sample was reduced down to 0.3 mW. The spectral data were collected in the 180° backscattering mode. Most attention was focused on the region from 2500 to 2900 cm^{-1} to monitor the CNT second order D*-band around 2690 cm^{-1}. The acquisition time varies between 60 and 300 s. Measurements were performed in situ at different temperatures.

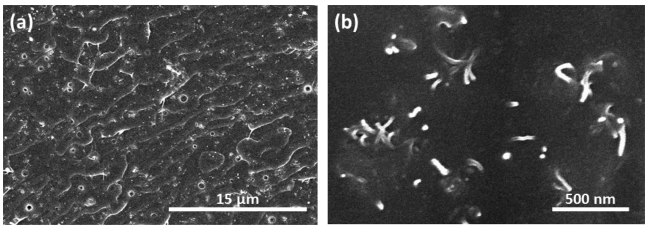

Figure 1. FE-SEM images of the fractured surface of NT1. The scale bar is (a) 15 μm and (b) 500 nm.

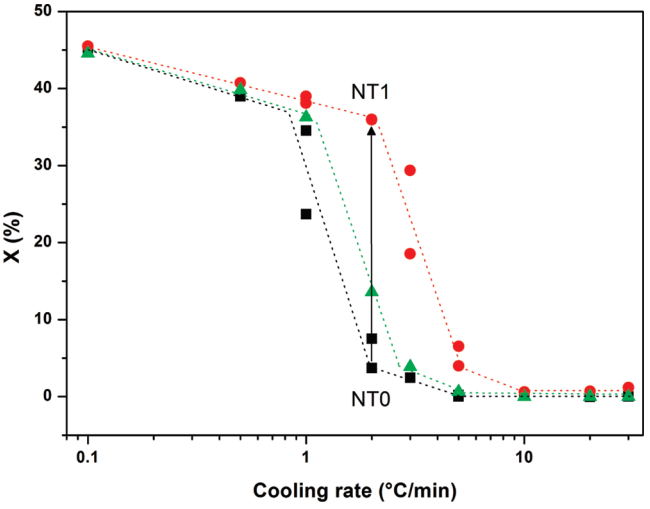

Figure 2. PLA crystal content versus cooling rate for NT0 (black squares), NT01 (green triangles), and NT1 (red circles).

3. RESULTS AND DISCUSSION

Assessment of the dispersion state of the CNTs in the polymer matrix is essential to understand the nanocomposite behavior. Figure 1 shows the SEM micrographs of NT1. CNT distribution in the polymer matrix appears fairly homogeneous at a few

micrometers scale (Figure 1a). However, at a scale lower than 0.5 μm, isolated CNTs as well as CNT bundles are seen on Figure 1b. Moreover, observations clearly suggest that nanotube bundles are indeed composite structures incorporating polymer, thus preserving a large interfacial area. It is worth noticing that the conductivity of NT1 is 1×10^{-5} S cm^{-1}, as measured from dielectric spectroscopy (Novocontrol), by contrast to 7×10^{-16} and 5×10^{-16} S cm^{-1} for NT01 and NT0, respectively. This means that CNTs are building up a percolating conduction network in the NT1 nanocomposite, in agreement with previous data from literature.[33]

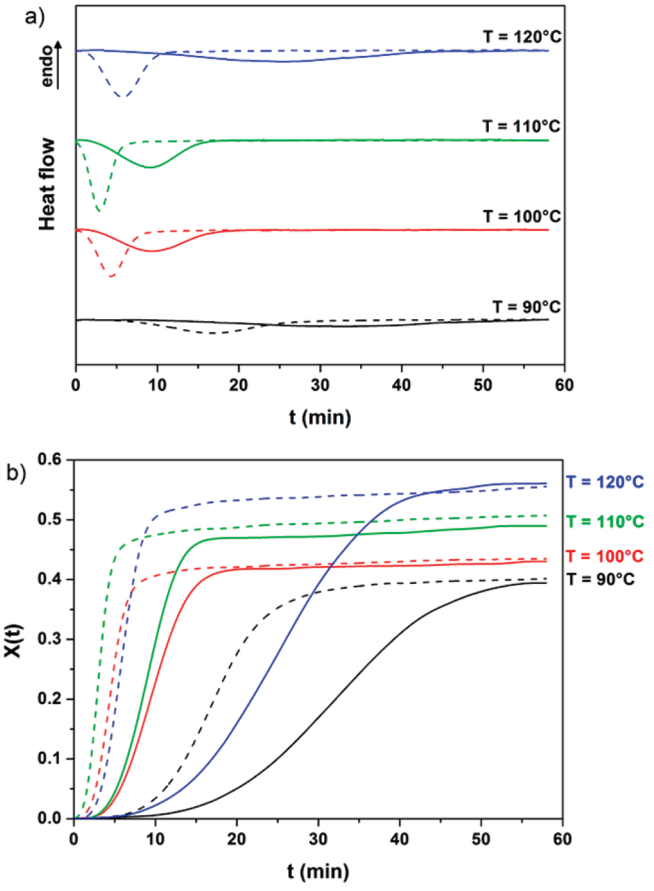

Figure 3. (a) Crystallization isotherms at various T_c for NT0 (solid line) and NT1 (dashed line) and (b) resulting crystallinity vs time.

Figure 2 presents the DSC cooling traces for nonisothermal crystallization of NT0 and nanocomposites NT01 and NT1 cooled from the melt at different rates. NT0 displays very slow crystallization kinetics. Optimum crystallinity close to 40% is reached when the cooling rate is decreased below 1 °C/min. Crystallinity is no more detectable for cooling rates greater than 5 °C/min. The presence of CNT impacts the crystallization kinetics of the PLA matrix. Crystal content reaches 5% with a cooling rate of 2 °C/min for NT0 while the same amount is obtained when the cooling rate is 3 and 5 °C/min for NT01 and NT1, respectively. Faster crystallization kinetics are achieved at increasing CNT content.

Isothermal crystallization has also been investigated for the various materials. The crystallization exotherms are reported in Figure 3a for four temperatures between 90 and 120 °C. Only NT0 and NT1 are presented for the sake of clarity. The time to reach the maximum degree of crystallization changes with temperature for both NT0 and NT1. An optimum in the crystallization kinetics appears for a temperature of 110 °C. This temperature corresponds to a compromise between nucleation and growth of crystals: crystal nucleation is favored at low temperature when molecular mobility is low, whereas crystal growth is favored at high temperature when viscosity is low. In the presence of CNTs, the crystallization exotherm of the PLA matrix increases in amplitude and sharpens. This means that either crystal nucleation or crystal growth of the PLA matrix is improved or both. Moreover, the time for crystallization completion is reduced, e.g., from 17 min for NT0 to 8 min for NT1 at 110 °C. The effect is even more pronounced at other temperatures when crystallization kinetics is slower.

Further analysis of the crystallization kinetics is provided by Figure 3b which reports the crystal weight fraction $X(t)$ vs time for NT0 and NT1. Each curve exhibits a sigmoid dependence on time. At the end of the $X(t)$ sigmoid evolution related to the completion of the primary crystallization stage, the faint increase in crystallinity may be attributed to a very slow secondary crystallization process. The time to reach the crystallinity "plateau" is shorter at 110 °C, for both NT0 and NT1, corroborating the previous finding that crystallization kinetics is optimum at this temperature. However, the maximum crystallinity of PLA, X_{max}, obtained after 60 min, steadily increases with temperature, irrespective of the optimum crystallization temperature. This points out the predominant role of crystal growth at high temperature. Besides, for each crystallization temperature, X_{max} in the nanocomposite is quasi-identical to that of the neat PLA.

Table 1. Avrami Coefficients for Isothermal Crystallizations and Glass Transition Temperature of the Amorphous Samples for Neat PLA and Nanocomposites

		T_c (°C)				
		90	100	110	120	T_g (°C)
NT0	K (min^{-n})	3.8×10^{-6}	4.9×10^{-4}	4.8×10^{-4}	2.3×10^{-5}	58.4
	n	3.5	3.2	3.3	3.2	
	$t_{1/2}$ (min)	31.9	9.7	9.1	25.2	
NT01	K (min^{-n})	6.1×10^{-6}	4.3×10^{-4}	8.8×10^{-4}	3.5×10^{-5}	59.3
	n	3.5	3.2	3.1	3.4	
	$t_{1/2}$ (min)	27.5	9.7	8.8	18.8	
NT1	K (min^{-n})	1.4×10^{-5}	5.5×10^{-3}	2.7×10^{-2}	1.7×10^{-3}	59.6
	n	3.8	3.2	2.8	3.4	
	$t_{1/2}$ (min)	17.2	4.5	3.1	5.9	

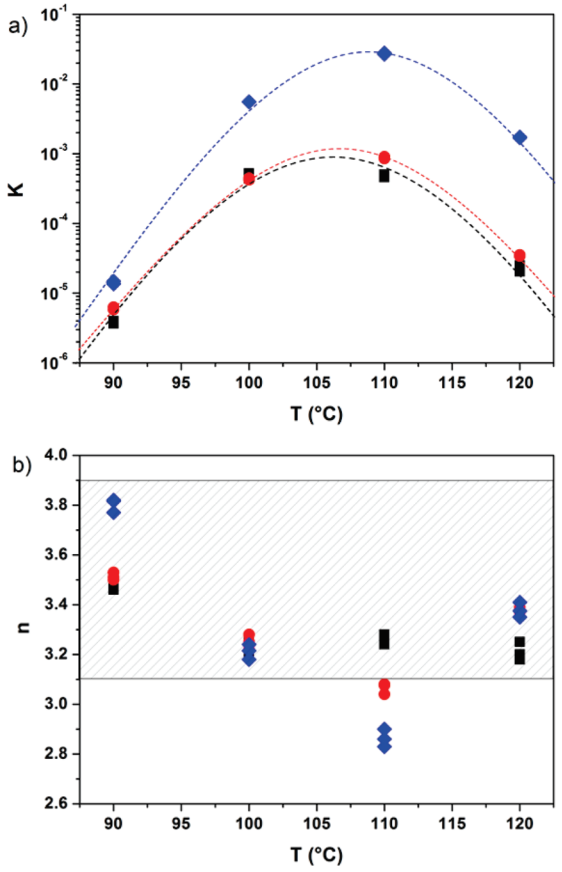

Figure 4. Evolution of (a) Avrami parameter K and (b) Avrami exponent n versus crystallization temperature for NT0 (black squares), NT01 (red circles), and NT1 (blue rhombs).

CNT incorporation influences the crystallization kinetics but does not affect the optimum crystallinity after 60 min isothermal crystallization. This suggests that CNTs have little effect on crystal growth, which means that nucleation should be the more CNT sensitive parameter.

From the time t_0 of the crystallization onset, the so-called induction time can be estimated. At T = 120 °C, t_0 = 3.5 min for NT0 and t_0 = 0.6 min for NT1. The t_0 value for nanocomposite is always lower than that of neat PLA. This is an additional hint that CNTs have a predominant effect on the crystal nucleation of the PLA matrix in the nanocomposites.

Avrami's theory is applied to analyze the isothermal crystallization of PLA and its composites in order to progress into understanding the role of CNTs on the nucleation and/or the growth of the PLA crystallites. The Avrami equation is given in eq 1

$$X(t) = 1 - \exp(-Kt^n) \quad (1)$$

with K a constant dependent on nucleation and growth parameters and n the Avrami exponent which depends on nucleation mechanisms and on crystal growth geometry. The values deduced for n and K parameters are summarized in Table 1.

The K constant is strongly temperature dependent. Figure 4a shows evolution of K with temperature and CNT content. Gaussian functions were used to fit the data. The crystallization kinetics is faster at higher CNT content. K values increase by as much as 1 order of magnitude or higher for the nanotube content

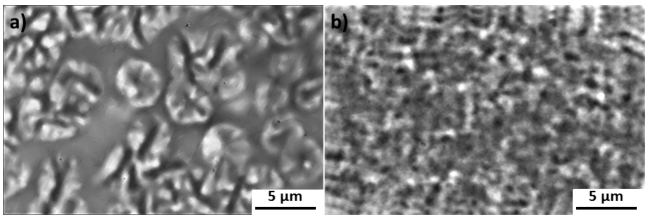

Figure 5. Optical micrographs of (a) NT0 and (b) NT1 after isothermal crystallization at T_c = 110 °C for 20 min.

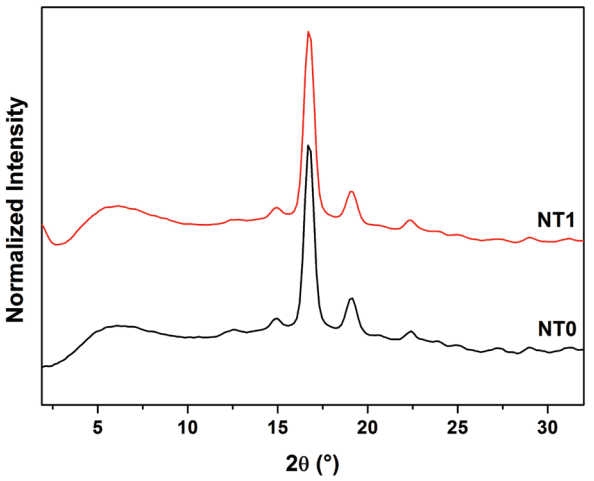

Figure 6. WAXS intensity profiles for NT0 and NT1 after crystallization at T = 120 °C for 2 h (λ = 1.54 Å).

under study. Moreover, the temperature for which the crystallization kinetics is the fastest increases with CNT content. The figure supports the conclusion from a previous work that kinetics of isothermal crystallization of neat PLA is optimum at 105 °C.[34] The optimum kinetics is slightly shifted up to 110 °C for NT1.

Evolution of the Avrami exponent is reported in Figure 4b. The n value between 3.1 and 3.9 is associated with a spherulitic growth (3D) from instantaneous (n = 3) and/or sporadic nuclei (n = 4). The addition of CNTs influences the PLA crystallization mechanism which is predominant at T = 110 °C. At this temperature, the Avrami exponent is 3.1 and 2.8 for NT01 and NT1, respectively. This temperature corresponds to an optimum for which the growth between 2D and 3D is induced from instantaneous nuclei (n = 2−3) and/or sporadic nuclei (n = 3).

The crystallization half-time is related to the n and K parameters after eq 2

$$t_{1/2} = (\ln 2/K)^n \quad (2)$$

where $t_{1/2}$ is the time at which the extent of relative crystallization is 50%. The values reported in Table 1 match those taken from Figure 3b (half-transformation). For all temperatures, the PLA crystallization half-time is higher than the one of the composites: $t_{1/2}$(NT0) > $t_{1/2}$(NT01) > $t_{1/2}$(NT1).

The crystallization behavior was followed up with polarized optical microscopy. The spherulitic morphology obtained after isothermal crystallization from melt state is shown in Figure 5. In the absence of nanotubes, PLA forms large spherulites with a size of ∼3−5 μm. By contrast, the crystal structure in the nanocomposite NT1 consists of smaller morphologies (<1 μm) for which the nature of contrast remains rather puzzling.

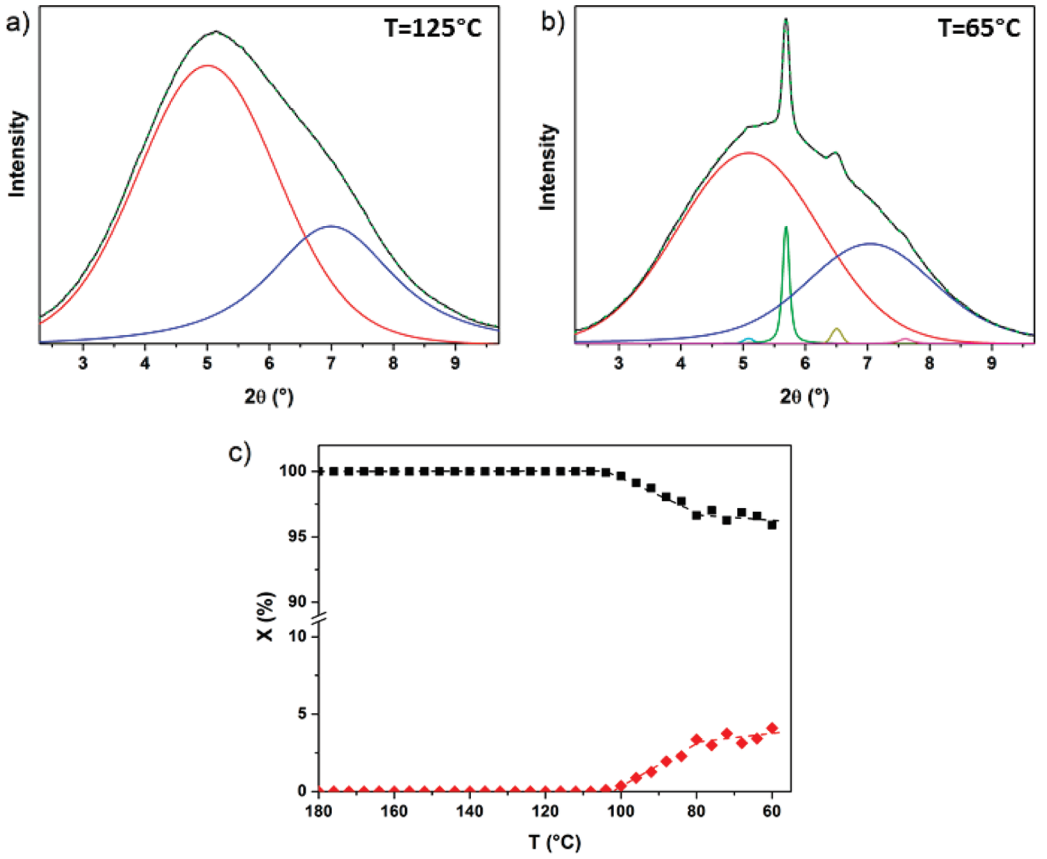

Figure 7. In-situ WAXS analysis (λ = 0.51 Å) of the PLA structure in NT1 as a function of temperature during anisothermal crystallization at a cooling rate of 5 °C/min: (a) WAXS profile at T = 125 °C and (b) at T = 65 °C and (c) crystallinity evaluated from crystalline (red rhombs) to amorphous (black squares) phase ratio.

Glass transition temperature values (T_g), measured prior to crystallization, are also shown in Table 1. A very small difference only appears in the T_g of PLA and nanocomposites. The values are close to 59 °C. The addition of CNTs induces no measurable change in the glass temperature transition.

The crystalline structure was checked by WAXS. Polymer crystallization was induced from the solid state by an annealing of 2 h at 120 °C. In general, depending on the preparation conditions, two different crystal structures α and β[35] may be obtained for PLA. Figure 6 shows the X-ray diffraction profile of the NT0 and NT1 materials. Structural analysis indicates that the polymer displays the orthorhombic α-crystalline form. The most intense peak is observed at 2θ = 16.7° due to reflections from (110) and (200) planes. Less intense peaks are also present at 2θ = 14.9°, 19.1°, and 22.4°, corresponding respectively to the reflections of (010), (203), and (210) planes. NT1 exhibits diffraction peaks located at the same 2θ positions. The incorporation of 1 wt % of CNTs does not modify the crystalline structure of PLA. The only difference in diffraction profiles is observed at very small angles and is related to a contribution of CNT nanofiller scattering.

In-situ WAXS experiments were also performed at ESRF during cooling from 180 °C to ambient temperature at 5 °C/min. As indicated in Figure 2, this cooling rate corresponds to a situation in which the composite is able to crystallize while the neat polymer cannot. The WAXS spectra were fitted by Gaussian functions to extract the fractions of amorphous and crystalline phases. Figures 7a and 7b show the profiles of the patterns recorded for two different temperatures (T = 125 and 65 °C, respectively). At T = 125 °C, profile fitting displays two amorphous contributions (broad peaks) located at 2θ = 5° and 2θ = 7°. The origin of these contributions is related to two characteristic intra- and interchain spacings in amorphous PLA.[36] The polymer matrix of NT1 is totally amorphous. In contrast, at T = 65 °C, the appearance of sharp peaks are indicative of the presence of the crystalline α-phase. The position of crystalline peaks does not vary upon cooling, indicating that the structure is not modified. The degree of crystallinity was calculated from the ratio of the crystalline to the amorphous phase contributions to the WAXS profiles. Figure 7c shows the evolution of crystal content versus temperature. Polymer crystallization starts at a temperature of 100 °C, and the crystallinity reaches 4% below 60 °C. These results are similar to those obtained by DSC.

Raman spectroscopy has proved to be a very useful technique for characterizing the structural properties and local environment of CNTs.[37−39] It was used to probe CNT−polymer interactions through CNT Raman signature. The Raman spectrum of CNT presents several characteristic bands. The disorder-induced D*-band which is directly related to the G-band (band of graphene)[40] is analyzed in the following. Figure 8a shows the NT1 Raman spectra during in-situ temperature scan experiments. The D*-bands were fitted by using a combination of Gaussian and Lorentzian functions. The bandwidths are equivalent, indicating that the matrix state changes only influence the global vibrational response. The difference in behavior is only characterized by the D*-band shift. The resulting wavenumber

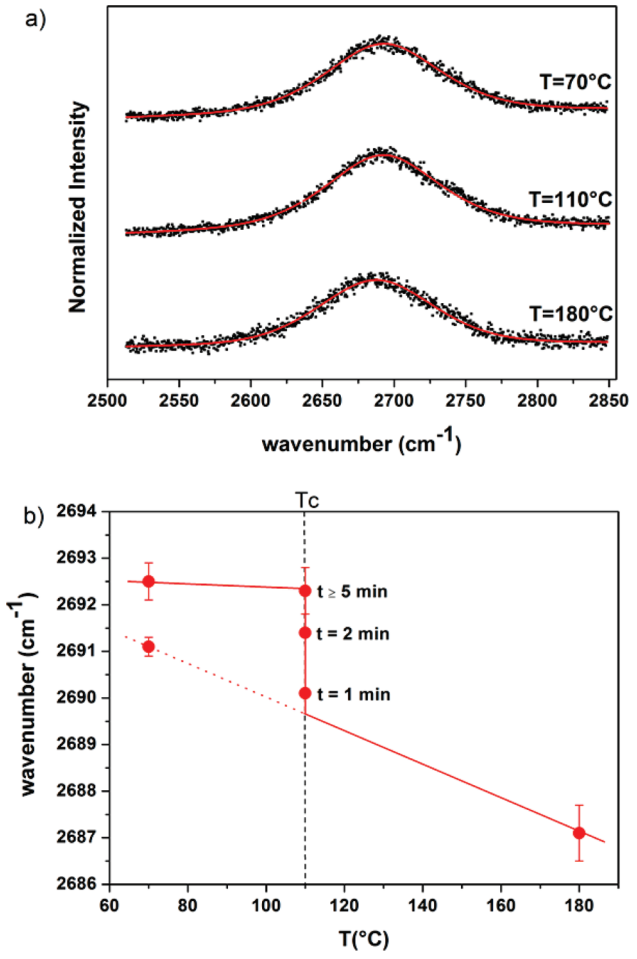

Figure 8. (a) Nanotube D*-band in the Raman spectra of NT1 composite and (b) evolution of the band wavenumber vs temperature.

evolution is reported in Figure 8b for NT1. At 180 °C, the PLA matrix is in the melt state. The average CNT wavenumber value is 2687.1 cm^{-1}. The polymer matrix is then allowed to crystallize at T_c = 110 °C. The amorphous phase remains in a constrained liquid state. The CNT wavenumber shifts with time and reaches a value of 2692.3 cm^{-1} after 5 min. Matrix crystallization at T_c = 110 °C implies a shift to a higher wavenumber (blue-shift) of the Raman peak, corresponding to a compressive stress on the CNTs.[41] Indeed, the frequency position of Raman peaks is sensitive to the local elastic deformation. When a strain is applied to a material, the interatomic distances change, and thus the vibrational frequencies of some of the normal modes change causing a Raman peak shift. At the very early stage of the crystallization process the nanotube vibrations are significantly affected which should not have occurred if the nucleation sites were located in the bulk polymer matrix. We may expect the polymer crystalline phase restricts the CNT vibrations.

Modification of the crystallization kinetics of the PLA matrix via introduction of CNTs appears in a reliable way on the cooling rate and the Avrami coefficients. These parameters all point at an evolution in the crystallization kinetics, which is explained by an increase of nucleation and/or growth of crystalline domains. The same glass transition temperature for the different samples means that for a given crystallization temperature the local chain motions in the amorphous phase are not significantly affected by the presence of CNTs, and thus the growth kinetics are identical. The difference in crystallization kinetic is then associated with a difference in the nucleation behavior between neat PLA and nanocomposites. The K exponent evolution with temperature indicates that nanotubes nucleate crystallization with only 1 wt %. Otherwise, Raman spectroscopy experiments are strongly indicative of the fact that CNTs act as nucleating agents in the nanocomposite. The high specific surface of nanotubes implies a large number of nucleation sites. The sporadic growth can be induced by CNT surface state and/or presence of defects. Mathew et al.[22] show that the filler surface topography is a decisive factor on crystallinity development. CNTs tend to promote transcrystallization of PLA with no change in crystalline structure. The actual local organization still remains to be elucidated.

4. CONCLUSION

In the present study, the crystallization kinetics of neat PLA and nanocomposites (NT01 and NT1) was explored in detail. In a first step, nanocomposite elaboration was optimized by solution and melt mixing in order to obtain a homogeneous dispersion of CNTs in the polymer matrix, as observed by FE-SEM. Calorimetric characterization of the nonisothermal and isothermal crystallization indicates the presence of CNTs significantly increases the crystallization kinetics of the PLA matrix. While the localized mobilities defined from T_g are similar, the difference in behavior is attributed to a nucleation activity of the nanofillers. In-situ Raman spectroscopy experiments corroborate such interpretation. The PLA isothermal crystallization at T_c = 110 °C displays a compression of the nanotubes by the polymer matrix compared to the melt state. At this temperature the nanotube vibrations are strongly affected by the crystalline phase, suggesting nucleation by CNTs. Nanofillers increase the number of nucleation sites and thereby decrease the average crystallite size as observed by optical microscopy. The corresponding nanocomposite crystalline structure, observed by X-ray scattering, is identical to that of semicrystalline neat PLA.

AUTHOR INFORMATION

Corresponding Author

*E-mail: sophie.barrau@univ-lille1.fr.

ACKNOWLEDGMENT

The authors are indebted to the Conseil Regional du Nord-Pas de Calais and the European Regional Development Fund (ERDF) for funding to the FE-SEM and WAXS equipment. The European Synchrotron Radiation Facility (Grenoble, France) is gratefully acknowledged for time allocation on the BM02 beamline as well as Dr. Cyrille Rochas for technical support.

REFERENCES

(1) Taylor, M. S.; Daniels, A. U.; Andriano, K. P.; Heller, J. *J. Appl. Biomater.* **1994**, *5*, 151–157.
(2) Drumright, R. E.; Gruber, P. R.; Henton, D. E. *Adv. Mater.* **2000**, *12*, 1841–1846.
(3) Södergård, A.; Stolt, M. *Prog. Polym. Sci.* **2002**, *27*, 1123–1163.
(4) Urayama, H.; Ma, C.; Kimura, Y. *Macromol. Mater. Eng.* **2003**, *288*, 562–568.
(5) Ray, S. S.; Yamada, K.; Okamoto, M.; Ueda, K. *Nano Lett.* **2002**, *2*, 1093–1096.

(6) Wu, D.; Wu, L.; Wu, L.; Xu, B.; Zhang, Y.; Zhang, M. *J. Polym. Sci., Part B: Polym. Phys.* **2007**, *45*, 1100–1113.
(7) Krikorian, V.; Pochan, D. J. *Macromolecules* **2005**, *38*, 6520–6527.
(8) Bordes, P.; Pollet, E.; Avérous, L. *Prog. Polym. Sci.* **2009**, *34*, 125–155.
(9) Pluta, M.; Galeski, A.; Alexandre, M.; Paul, M.-A.; Dubois, P. *J. Appl. Polym. Sci.* **2002**, *86*, 1497–1506.
(10) Oksman, K.; Skrifvars, M.; Selin, J.-F. *Compos. Sci. Technol.* **2003**, *63*, 1317–1324.
(11) Samir, A. S. A.; Alloin, F.; Dufresne, A. *Biomacromolecules* **2005**, *6*, 612–626.
(12) Murariu, M.; Dechief, A. L.; Bonnaud, L.; Paint, Y.; Gallos, A.; Fontaine, G.; Bourbigot, S.; Dubois, P. *Polym. Degrad. Stab.* **2010**, *95*, 889–900.
(13) Bourbigot, S.; Fontaine, G. *Polym. Chem.* **2010**, 1413–1422.
(14) Xu, J.-Z.; Chen, T.; Yang, C.-L.; Li, Z.-M.; Mao, Y.-M.; Zeng, B.-Q.; Hsiao, B. S. *Macromolecules* **2010**, *43*, 5000–5008.
(15) Schadler, L. S.; Giannaris, S. C.; Ajayan, P. M. *Appl. Phys. Lett.* **1998**, *73*, 3842–3844.
(16) Coleman, J. N.; Khan, U.; Blau, W. J.; Gun'ko, Y. K. *Carbon* **2006**, *44*, 1624–1652.
(17) Barrau, S.; Demont, P.; Peigney, A.; Laurent, C.; Lacabanne, C. *Macromolecules* **2003**, *36*, 5187–5194.
(18) Sahoo, N. G.; Rana, S.; Cho, J. W.; Li, L.; Chan, S. H. *Prog. Polym. Sci.* **2010**, *35*, 837–867.
(19) Miyata, T.; Masuko, T. *Polymer* **1998**, *39*, 5515–5521.
(20) Na, B.; Tian, N.; Lv, R.; Li, Z.; Xu, W.; Fu, Q. *Polymer* **2010**, *51*, 563–567.
(21) Papageorgiou, G. Z.; Achilias, D. S.; Nanaki, S.; Beslikas, T.; Bikiaris, D. *Thermochim. Acta* **2010**, *511*, 129–139.
(22) Mathew, A. P.; Oksman, K.; Sain, M. *J. Appl. Polym. Sci.* **2006**, *101*, 300–310.
(23) Wu, D.; Wu, L.; Zhou, W.; Zhang, M.; Yang, T. *Polym. Eng. Sci.* **2010**, *50*, 1721–1733.
(24) Vega, J. F.; Martinez-Salazar, J.; Trujillo, M.; Arnal, M. L.; Muller, A. J.; Bredeau, S.; Dubois, P. *Macromolecules* **2009**, *42*, 4719–4727.
(25) Li, J.; Fang, Z.; Zhu, Y.; Tong, L.; Gu, A.; Liu, F. *J. Appl. Polym. Sci.* **2007**, *105*, 3531–3542.
(26) Bhattacharyya, A. R.; Sreekumar, T. V.; Liu, T.; Kumar, S.; Ericson, L. M.; Hauge, R. H.; Smalley, R. E. *Polymer* **2003**, *44*, 2373–2377.
(27) Haggenmueller, R.; Fischer, J. E.; Winey, K. I. *Macromolecules* **2006**, *39*, 2964–2971.
(28) Brosse, A.-C.; Tence-Girault, S.; Piccione, P. M.; Leibler, L. *Polymer* **2008**, *49*, 4680–4686.
(29) Grady, B. P.; Pompeo, F.; Shambaugh, R. L.; Resasco, D. E. *J. Phys. Chem. B* **2002**, *106*, 5852–5858.
(30) Wu, D.; Wu, L.; Sun, Y.; Zhang, M. *J. Polym. Sci., Part B: Polym. Phys.* **2007**, *45*, 3137–3147.
(31) Fisher, E.; Sterzel, H. J.; Wegner, G. *Kolloid Z. Z. Polym.* **1973**, *251*, 980–990.
(32) Hammersley, A. P. "FIT2D V9.129 Reference manual v3.1, ESRF report 98HA01T", 1998.
(33) Yoon, J. T.; Jeong, Y. G.; Lee, S. C.; Min, B. G. *Polym. Adv. Technol.* **2009**, *20*, 631–638.
(34) Stoclet, G.; Elkoun, S.; Miri, V.; Séguéla, R.; Lefebvre, J.-M. *International Polymer Processing XXII* **2007**, *5*.
(35) Hoogsteen, W.; Postema, A. R.; Pennings, A. J.; Brinke, G. T. *Macromolecules* **1990**, *23*, 634–642.
(36) Stoclet, G.; Seguela, R.; Lefebvre, J. M.; Elkoun, S.; Vanmansart, C. *Macromolecules* **2010**, *43*, 1488–1498.
(37) Wood, J. R.; Zhao, Q.; Wagner, H. D. *Composites, Part A* **2001**, *32*, 391–399.
(38) Dresselhaus, M. S.; Dresselhaus, G.; Saito, R.; Jorio, A. *Phys. Rep.* **2005**, *409*, 47–99.
(39) Bassil, A.; Puech, P.; Landa, G.; Bacsa, W.; Barrau, S.; Demont, P.; Lacabanne, C.; Perez, E.; Bacsa, R.; Flahaut, E.; Peigney, A.; Laurent, C. *J. Appl. Phys.* **2005**, *97*, 034303.
(40) Matthews, M. J.; Pimenta, M. A.; Dresselhaus, G.; Dresselhaus, M. S.; Endo, M. *Phys. Rev. B* **1999**, *59*, R6585.
(41) Ruan, S. L.; Gao, P.; Yang, X. G.; Yu, T. X. *Polymer* **2003**, *44*, 5643–5654.